SYNTHESIS OF A NOVEL BIOBASED AND PHOTOCURABLE VITRIMER [redacted]

Bachelor's Thesis

Degree in Chemistry

Academic tutor: Dra. Anna Maria Masdeu

Company tutor: Dr. Pere Manel Verdugo

Josep Benet Piñero Navarro

June 2025

ACKNOWLEDGEMENTS

This research work would not have been possible without the help and guidance of my supervisor, Dr. Pere Manel Verdugo and Dr. David Santiago who has also helped me a lot. I am very grateful to have been given this opportunity to experience the world of research in first person. Thank you for all the advice and support given throughout all this time.

On the other hand, I would like to thank all the members of Eurecat, especially, to the ones that I share laboratory with because we have created such a great atmosphere. Thank you for sharing with me all your knowledge, for your patience and for all your advice. I would also like to thank my colleagues Claudia Fontova and Ramon Messeguer, this time in Eurecat would not have been the same without you two.

Moreover, I would also like to thank the friends I have made along these years. We have cried and suffered but also laughed a lot. I am so grateful to have had the opportunity to meet you, and even though this journey comes to an end, the memories of all these years will be a part of me for the rest of my life.

Finally, this would not be a proper acknowledgement without mentioning my family, especial mention to my mother who is my entire life. To the rest of my family, thank you for always supporting me, I will be forever grateful for everything you have done for me during all these years.

TABLE OF CONTENTS

ABSTRACT

English:

This bachelor's work is designed to provide practical experience in research, particularly in the field of polymer synthesis and all its associated processes. It encompasses bibliographic research, calculations, reaction development, product purification, characterization, and result interpretation.

In this work, a biobased methacrylate monomer has been synthesized and subsequently reacted with another methacrylate monomer in the presence of a photoinitiator, leading to the formation of a vitrimeric material.

Various characterization techniques, including NMR and IR, have been employed to confirm that the desired material was successfully obtained. Additionally, other characterization techniques such as DMA and DSC among others have been very useful to assess the thermomechanical properties of the material or the glass transition temperature (T_g).

Català:

Aquesta treball de fi de grau està dissenyat per aportar experiència pràctica en el món de la recerca, especialment en el camp de la síntesi de polímers i tots els seus processos associats. Comprèn la recerca bibliogràfica, els càlculs, el desenvolupament de reaccions, la purificació del producte, la caracterització i la interpretació de resultats.

En aquest treball, s'ha sintetitzat un monòmer de metacrilat d'origen renovable i posteriorment s'ha fet reaccionar amb un altre monòmer de metacrilat en presència d'un fotoiniciador, donant lloc a la formació d'un material vitrimèric.

S'han emprat diverses tècniques de caracterització, incloent RMN i IR, per confirmar que el material desitjat s'ha obtingut amb èxit. A més, altres tècniques de caracterització com DMA i DSC entre d'altres han estat molt útils per avaluar les propietats termomecàniques del material o la temperatura de transició vítria (T_g).

1 OBJECTIVES

The objective of this work was to synthesize a novel photocurable methacrylate vitrimer derived from renewable resources.

2 DEVELOPMENT AREA

This work was carried out at the Chemical Technologies Unit of Eurecat, located in the industrial area, as part of an internal project focused on obtaining vitrimeric materials derived from natural sources.

CONFIDENTIALITY

The results of this work are susceptible to be patented, for which a confidentiality agreement has been signed between the Rovira and Virgili University and Eurecat. Furthermore, in the public version, the results, synthetic routes and sensitive will be censored.

3 INTRODUCTION

The vast majority of organic chemicals and polymers are currently derived from fossil-based resources. However, as the demand for these non-renewable materials continues to rise, their depletion will lead to significant supply challenges, price increases, and unpredictable social repercussions. As a result, the search for sustainable alternatives sourced from biomass has become a priority. This has given rise to the concept of biorefinery, which aims to process each component of biomass into valuable products, much like crude oil refineries.

Although bio-based chemicals are already available industrially, most are aliphatic or cycloaliphatic, originating from sources such as cellulose, starch, or triglycerides. However, many crucial chemicals used in various industries are aromatic compounds traditionally derived from petroleum. In recent years, the surge in shale gas production—being lighter than petroleum—has led petrochemical industries to adapt their processes. This shift has resulted in a decline in the production of heavier coproducts such as aromatics, propylene, and butadiene, thereby reducing the availability and increasing the price of aromatic compounds.

To address this challenge, researchers are exploring biomass-derived alternatives to aromatic building blocks. In nature, aromatics primarily exist as polyphenolics, which can be obtained from renewable sources such as lignin, tannins (both extracted from wood), and cashew nutshell liquid (CNSL). Their relative commercial availability is shown in **Figure 1**.

Despite the abundance of polyphenolic materials, particularly lignin and tannins, their industrial application remains underdeveloped compared to aliphatic bioresources,

such as vegetable oils. This disparity can be attributed to processing challenges, variability in composition, and polymeric complexity, which hinder their direct use in large-scale applications.

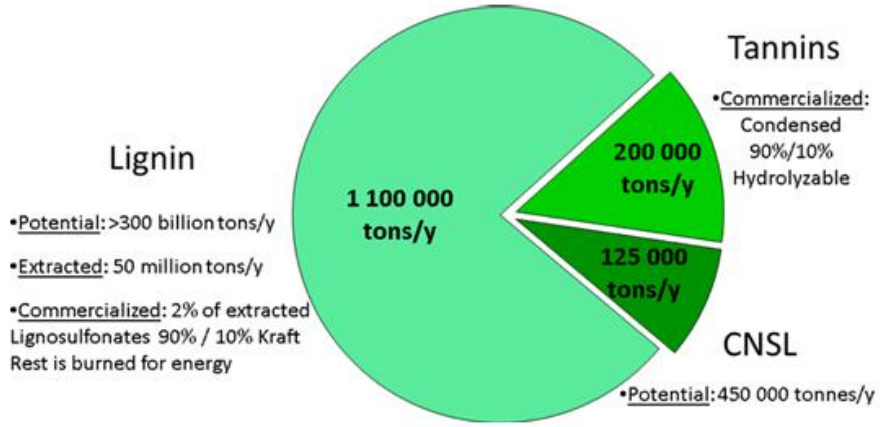

Figure 1. Commercial availability of lignin, tannins, and CNSL.[1]

A promising approach involves the depolymerization of lignin to obtain molecular aromatic compounds, such as ferulic acid and vanillin. Although ferulic acid can be sourced from rice bran, sugar cane bagasse, and sugar beet pulp, vanillin is the most commercially available monoaromatic phenol derived from lignin.[1]

3.1 VANILLIN

With an annual output of approximately 20,000 tons, including 3,000 tons from lignin, vanillin (**Figure 2**) is a promising renewable aromatic compound with strong potential for polymer applications. Its safety, stability, and versatile reactivity make it well-suited for polymer synthesis, offering a more manageable alternative to raw lignin, which is highly multifunctional and complex to process. Vanillin's difunctional nature facilitates chemical modifications, enhancing its utility in polymer production.

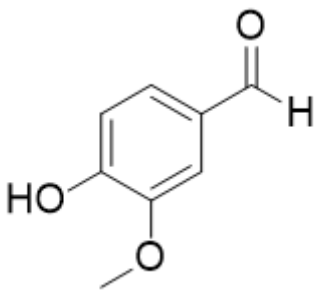

Figure 2. Vanillin's chemical structure

In **Figure 3** different vanillin derivatives can be observed.

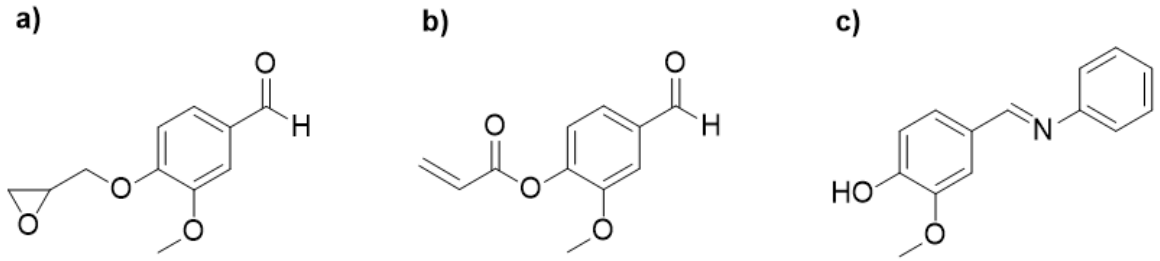

Figure 3. Structures of different vanillin derivatives. a) Vanillin diglycidyl ether b) Vanillin acrylate c) Vanillin Schiff base

Moreover, its lignin-derived origin ensures sustainability without competing with food resources, reinforcing its viability as an environmentally responsible feedstock. Its wide-ranging benefits make it a strong candidate for replacing conventional petrochemical-derived aromatic monomers.

From an economic standpoint, vanillin sourced from lignin remains competitive. The established lignin-to-vanillin process, utilizing lignosulfonates, has contributed to vanillin's position as one of the few molecular phenolic compounds industrially produced from biomass. Given the crucial role of aromatic monomers in achieving desirable mechanical and thermal properties in polymers, ongoing research continues to highlight its significance in sustainable chemistry. Rising petroleum costs, advancements in production efficiency, and improvements in waste reduction further strengthen its viability within green industry initiatives.

Beyond serving as a replacement for traditional petro-based aromatics, vanillin is also a foundation for pioneering polymer designs with distinct functional properties. These innovations extend to applications such as antimicrobial coatings films,[2] metal ion-chelating materials,[3] and liquid crystalline polymers,[4] demonstrating vanillin's versatility in sustainable materials development. [1]

Although using materials coming from renewable sources is a step toward sustainability, ensuring their recyclability and reprocessability is essential for advancing a circular economy and promoting greener chemistry. By prioritizing these qualities, materials can be continuously repurposed, minimizing waste and reducing environmental impact.

Recent advancements in polymer research focus on improving recyclability, particularly in thermosets, which have long been considered among the most difficult materials to recycle. Their covalent intermolecular cross-links enhance strength, stiffness, and resistance to creep, providing excellent thermal and chemical stability. These properties make thermosets the preferred choice for applications requiring durability, such as

aerospace structures and wind turbines. However, their permanent molecular architecture prevents reshaping, reprocessing, or recycling, posing a major challenge in sustainable material development. Addressing this issue is essential for creating more environmentally responsible polymers.[5–7]

In 2011, a new class of materials called vitrimers were introduced by Liebler and co-workers. Such materials have the remarkable property that they can be reprocessed without losing its network integrity.[6–8]

3.2 VITRIMERS

Vitrimers are a unique class of polymers that retain the outstanding properties of thermosets while overcoming their lack of reprocessability. This is achieved by the introduction of reversible exchangeable chemical bonds, leading to dynamic cross-links. If chemical cross-links can be efficiently and reliably exchanged between different positions of the organic polymer network, macroscopic flow can be achieved without risking structural damage or permanent loss of material properties.

Polymer networks containing such exchangeable bonds are also known as covalent adaptable networks or CANs. CAN enable reversible responses to external stimuli (**Figure 4**). In their dormant state, these networks behave like conventional thermosets with stable covalent bonds. However, when exposed to an appropriate stimulus, bond exchange facilitates polymer chain movement and network topology rearrangement, leading to macrostructural changes such as stress relaxation, reprocessing, reshaping and so on. Once the stimulus is removed, the material returns to its original thermoset state, ensuring durability while allowing adaptability.[8,11]

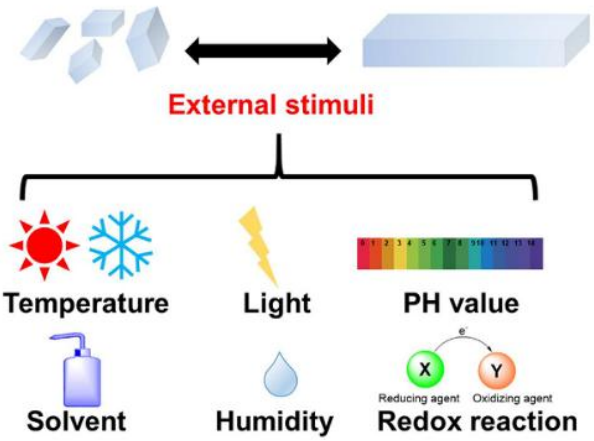

Figure 4. External stimuli used to trigger the reversible bonds in CANs.[8]

CANs may be classified into two groups depending on their exchange mechanism.

The first group of CANs makes use of a dissociative cross-link exchange mechanism (**Figure 5-A**). In this exchange, the original chemical bond is first broken before the new bond is formed, therefore, the structural integrity of the network is lost.

The second group of CANs makes use of associative bond exchanges between polymer chains (**Figure 5-B**), in which the new bond is formed simultaneously when the original bond is broken, it results in a minimal change in macromolecular structure during their bond exchange and the degree of crosslinking is maintained during the bond exchange.[11] Vitrimers are characterized by their associative nature.

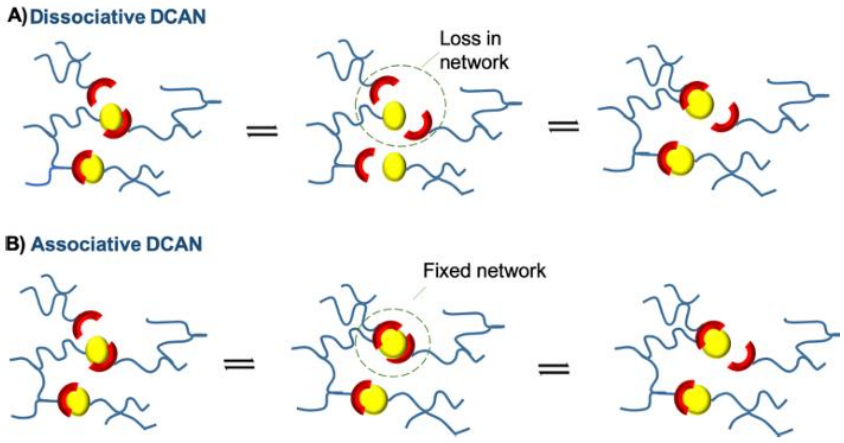

Figure 5. A) Dissociative exchange and B) Associative exchange in dynamic CANs.[11]

3.3 RADICAL POLYMERIZATION

Radical polymerization is a type of chain-growth polymerization that occurs through the formation of reactive radicals. The process consists of three main stages: initiation, propagation, and termination. Various initiation methods exist, including thermal, photochemical, and redox initiation. Thermal initiation generates radicals by applying heat to the initiator, while photochemical initiation involves excitation by

electromagnetic radiation, leading to radical formation as the initiator returns to its ground state.

Radical polymerization begins with initiation, where the initiator undergoes homolytic cleavage, generating two radicals. These radicals react with the vinylic part of a monomer, forming a new radical that enters to the propagation stage. During propagation, this radical continuously reacts with additional vinylic monomers, theoretically persisting until all monomer is consumed. The final stage, termination, can occur through combination, disproportion, or chain transfer. In the case of combination, two growing polymer chains merge, by combining their radicals. In the disproportion, one radical from one chain abstracts a hydrogen atom from the other chain, giving rise to one saturated and one unsaturated chain. Finally, in chain transfer, instead of eliminating, the radical is transferred to another molecule allowing the polymerization process to restart.

A schematic representation of the different stages found in free radical polymerization are shown in **Scheme 1**.

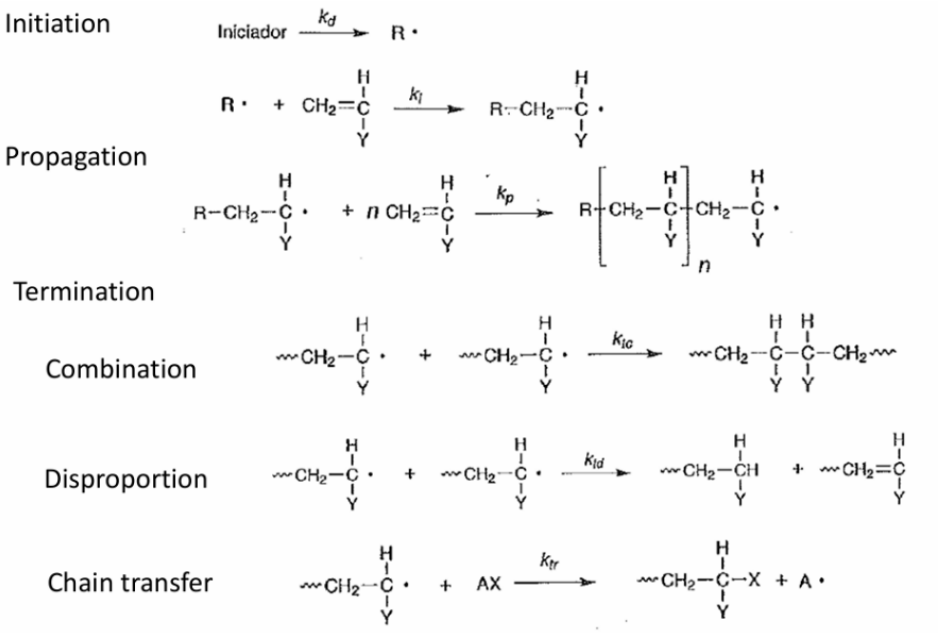

Scheme 1. Stages of free radical polymerization.

4 EXPERIMENTAL PART

4.1 REAGENTS AND SOLVENTS USED

In **Table 1**, the most relevant data related to the toxicity and purity of the reagents and solvents used in the synthesis of the different products is presented.

Table 1. Toxicity and purity data of reagents and solvents

REAGENTS	PURITY	TOXICITY
Vanillin	99%	
[redacted]	98%	
[redacted]	≥99%	Not classified for physical or health hazards under GHS
Methacryloyl chloride	97%	
Triethylamine	≥99.5%	
[redacted]	≥92%	
4-(dimethylamino)pyridine	≥99%	
Methacrylic acid	99.5%	
Thionyl chloride	97%	
Hydroquinone	≥99%	
Guaiacol	≥98%	
2,4-Di-tert-butylphenol	99%	
Sodium hydroxide	≥98%	
$NaHCO_3$	≥99.7%	Not classified for physical or health hazards under GHS
HCl	37%	

Phenylbis(2,4,6-trimethylbenzoyl)-phosphine oxide	>95%	
Methanesulfonic acid	99%	

SOLVENTS	PURITY	TOXICITY
H_2O	Milli-Q	Not classified for physical or health hazards under GHS
CH_2Cl_2	≥99.9%	
Ethyl acetate	≥99.5%	
Hexane	≥99.9%	
EtOH	≥99.5%	
Tetrahydrofuran	≥99.9%	

The explanation of the meaning of each pictogram can be found in https://echa.europa.eu/es/regulations/clp/clp-pictograms

4.2 EXPERIMENTAL PART

4.2.1 Synthesis of vanillyloxime (VanOx)

[redacted]

As a typical example, 18.00 g (259.03 mmol) of [redacted] and 64.40 g (473.25 mmol) of [redacted] were introduced into a 500 mL round-bottom flask and were solubilized in 360 mL of distilled water. Then, 36.00 g (236.61 mmol) of vanillin was added. The mixture was heated at 100 ºC for 1 hour until a clear solution was

obtained. The reaction mixture was left to cool down to room temperature and the product precipitated as white crystals. The crystals were filtered, washed with cold water, and dried in a vacuum oven at 40 ºC overnight, obtaining an 83% yield of pure product.

[redacted]

4.2.2 Synthesis of methacryloyl chloride

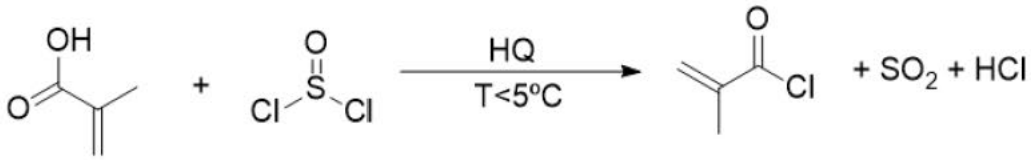

Scheme 3. Synthesis of methacryloyl chloride

Methacryloyl chloride was synthetized following a reported procedure.[13]

In a 250 mL round-bottomed flask equipped with a magnetic stir bar, 80.7 mL (1.11 mol) of thionyl chloride was added dropwise below 5ºC over 100 mL (1.19 mol) of methacrylic acid. After that, 0.30 g (2.7 mmol) of hydroquinone was added and the resultant mixture was stirred for 2 hours at room temperature. Subsequently, the reaction was heated at 50 °C for 2 h. After the reaction has been completed the product was isolated and purified by distillation. Pure methacryloyl chloride (70.13 mL, 84.9 %) was obtained at 92-97 °C.

^{1}H-NMR ($CDCl_3$, 400 MHz, TMS, δ ppm): 6.49 (s, 1H, -CH=C-), 6.03 (s, 1H, -CH=C-), 1.95 (s, 3H, -CH_3). (**Figure A3**)

4.2.3 Synthesis of [redacted]

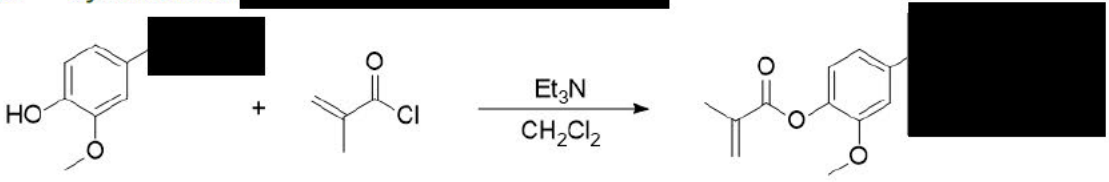

[redacted]

For the synthesis of [redacted] a reported procedure describe in the bibliography was followed.[14]

In a 500 mL round-bottomed flask equipped with a magnetic stir bar, 20.00 g of [redacted] (119.64 mmol) were added and solubilized in 200 mL of dry dichloromethane and then 35 mL of methacryloyl chloride (358.86 mmol) were added. The solution was cooled to 0ºC and a mixture of 50 mL triethylamine (358.73 mmol) in 133 mL of dichloromethane was added dropwise. The reaction was stirred for 30 minutes at 0ºC and then 30 minutes at room temperature. The progress of the reaction was monitored by ^{1}H NMR. After the reaction reached complete conversion, the organic layer was washed with 2 x 130 mL of distilled water, 1 x 130 mL of 5% bicarbonate solution, and 2 x 130 mL of saturated sodium chloride solution. After drying the organic layer over magnesium sulfate and filtration of the drying agent, the solvent was distilled off.

ESI-MS, exact mass m/z [M+H^{+}] = 304.1180 (theoretical mass: 304.1179).

[redacted]

4.2.4 Synthesis of guaiacol methacrylate (Meta-Guai)

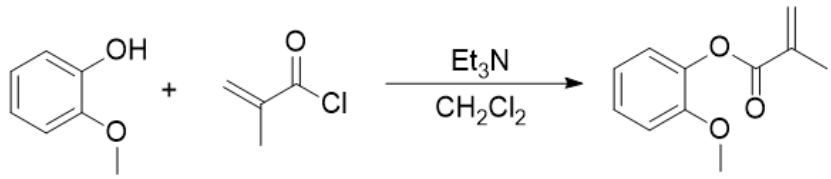

Scheme 5. Synthesis of guaiacol methacrylate

For the synthesis of guaiacol methacrylate (Meta-Guai) a reported procedure describe in the bibliography was followed.[14]

In a 1L round-bottomed flask equipped with a magnetic stir bar, 71.43 mL of guaiacol (80.64 g, 0.6546 mol) were added and dissolved in 300 mL of dry dichloromethane and then 95 mL of methacryloyl chloride (0.9724 mol) were added. The solution was cooled to 0ºC and a mixture of 135 mL triethylamine (0.9685 mol) in 170 mL of dichloromethane was added dropwise. The reaction was stirred for 30 minutes at 0ºC and then 30 minutes at room temperature. The progress of the reaction was monitored by ^{1}H NMR. After reaction was finished, the mixture was filtrated to eliminate the maximum possible salt, which was generated as a byproduct of the reaction and then the solvent was distilled off. As the product was liquid, after evaporating the solvent in the rotary evaporator a vacuum distillation was performed adding the 0.02 wt.% of 2.4-di-tert-butylphenol as

radical inhibitor. The product was obtained with a 50 % yield in the distillate at 83 ºC (0.5 mbar).

ESI-MS, exact mass m/z [M+H$^+$] = 193.0860 (theoretical mass: 193.0859).

^{1}H-NMR ($CDCl_3$, 400 MHz, TMS, δ ppm) : 7.21 (m, 1H, Ar.), 7.07 (dd, ^{3}J=7.6 Hz, ^{4}J=1.6 Hz 1H, Ar.), 6.98 (m, 2H, Ar.), 6.38 (m, 1H, -C=CH_2), 5.75 (m, 1H, -C=CH_2), 3.82 (s, 3H, CH_3-O-), 2.09 (m, 1H, CH_3-C). (**Figure A7**)

^{13}C-NMR ($CDCl_3$,100.6 MHz, TMS, δ ppm): 165.51 (-COO-), 151.36 (Ar.), 140.06 (Ar.), 135.73 (-C=CH_2), 127.16 (-C=CH_2), 126.85 (Ar.), 122.92 (Ar.), 120.82 (Ar.), 112,57 (Ar.), 55.94 (CH_3-O-), 18.51 (CH_3-C-). (**Figure A8**)

4.2.5 Preparation of the formulations

To prepare the formulations, the [redacted] was introduced into a vial and dissolved in guaiacol methacrylate (reactive diluent) with gentle heating to facilitate the dissolution. Then, 0.03 g of phenylbis(2,4,6-trimethylbenzoyl)-phosphine oxide (commonly known as BAPO) was added as photoinitiator. Using a syringe, the prepared formulations were then transferred into a Teflon mold (**Figure 6**) covered with two glass pieces and supported by metallic clamps (**Figure 7**).

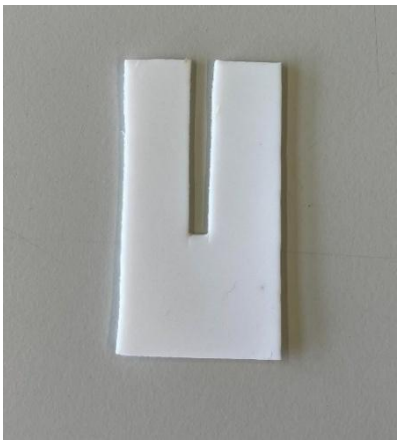

Figure 6. Teflon mold

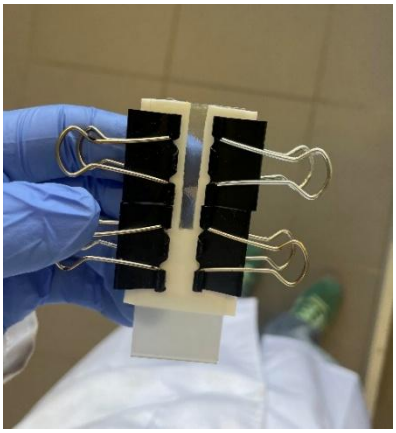

Figure 7. Set up.

The sample was subjected to UV light irradiation (between 365-405 nm) for five minutes, initiation the desired reaction and completing the process.

To make sure that the photopolymerization was done successfully an IR analysis of the material was done before and after the photopolymerization step (**Figure 8**).

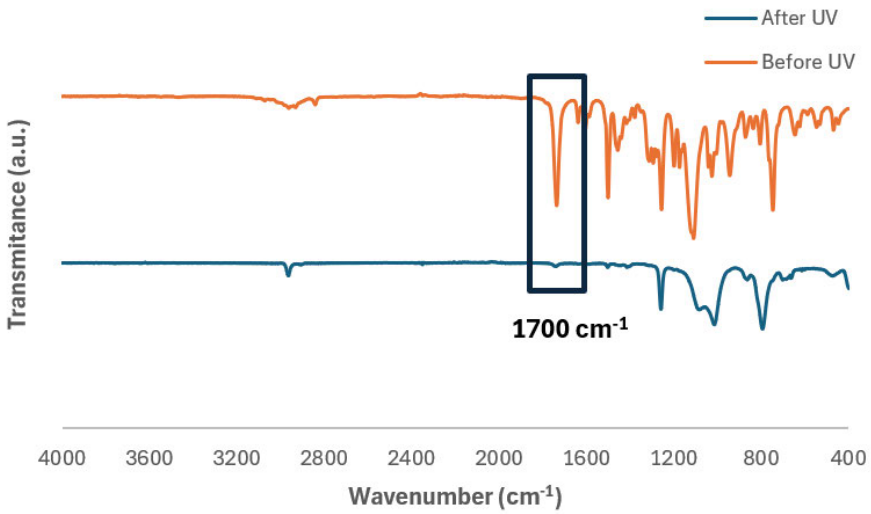

Figure 8. IR spectrum before and after photopolymerization

[redacted].

Finally, a post curing treatment was performed at 160ºC for 1 hour.

In **Table 2** the different prepared formulations with the corresponding weighted amounts can be seen.

[redacted]

4.2.6 Gel fraction

The gel fraction technique is used to quantify the insoluble portion of a crosslinked polymer network, specifically the fraction that remains after solvent extraction. This measurement reflects the degree of crosslinking, indicating how much of the material forms a three-dimensional network that cannot dissolve in a solvent. To determine the gel fraction, a material sample was firstly weighed to obtain its initial dry mass. It is then immersed in an appropriate solvent, in our case the solvent used was tetrahydrofuran because it's a solvent in which the monomer or the non-crosslinked polymers are initially soluble and do not react with the exchangeable functions allowing the extraction of the soluble, non-crosslinked polymer chains, known as the sol fraction, while the

crosslinked network remains intact. After soaking, the sample is removed, dried in a vacuum oven to eliminate residual solvent, and reweighed. The gel fraction is then calculated as the ratio of the final dry mass (m_2) to the initial dry mass (m_1) and it is expressed as a percentage.[6]

In **Table 3**, the different gel fraction parameters for each formulation can be seen.

Table 3. Gel fraction parameters

[redacted]	THF volume	m_0	m_2	GF (%)
	18 mL	0.2977 g	0.2819 g	94.6%
	18 mL	0.2595 g	0.2456 g	94.6%
	18 mL	0.2934 g	0.1588 g	54.1%

From the results obtained in **Table 3**, two clear different results can be distinguished.

On one hand, formulations 20/80 and 25/75 yielded a gel fraction of 94.6% indicating a dense and well-developed polymer network with strong mechanical integrity, low solubility, and enhanced chemical resistance.

On the other hand, formulation 30/70 yielded a gel fraction of 54.1%, a notably low value compared to the other formulations. [redacted]

4.3 CHARACTERITZATION TECHNIQUES

4.3.1 Differential Scanning Colorimetry (DSC)

Differential scanning calorimetry was used for thermal characterization with the Mettler-Toledo DSC3+ instrument (**Figure 9**). Indium standards were employed for the heat flow calibration, while zinc standards were used for temperature calibration.

Glass transition temperature (T_g) and melting temperatures (T_m) values were obtained from approximately 10 mg samples using aluminium crucibles under a nitrogen flow of 50 mL·min^{-1}. The results are presented as heat flow (W·g^{-1}) vs temperature (ºC).

T_g analyses were conducted within a temperature range of -20ºC to 180ºC, while melting measurements were performed between -10ºC and 120ºC.

Figure 9. Mettler-Toledo DSC3+

4.3.2 Nuclear Magnetic Resonance Spectroscopy (NMR)

This technique was used to characterize the obtained products. The analysis was performed using a Varian VNMR-S400 NMR spectrometer (**Figure 10**) (Agilent Technologies, Santa Clara, CA, USA), providing ^{1}H,^{13}C, HMBC and HSQC spectra.

Figure 10. Varian VNMR-S400 NMR spectrometer

Deuterated chloroform ($CDCl_3$) was used in some analysis as solvent and the provided results are reported in parts per million (ppm) with the residual solvent peak serving as a reference (^{1}H NMR: $CDCl_3$= 7.26 ppm; ^{13}C NMR: $CDCl_3$= 77.16 ppm). DMSO-d_6 was also used as a deuterated solvent for some analysis the results are also reported in parts per million (ppm) with the residual peak serving as a reference (^{1}H NMR: DMSO-d_6= 2.50 ppm; ^{13}C NMR: DMSO-d_6= 39.52 ppm).

4.3.3 Thermogravimetric analysis (TGA)

Thermogravimetric analysis was used to evaluate the thermal stability of the materials. The instrument employed was a Mettler Toledo TGA2 thermobalance (**Figure 11**). Sample weight loss was measured over a temperature range of 30ºC to 600ºC at a heating rate of 10ºC·min^{-1} under a nitrogen atmosphere.

Figure 11. Mettler Toledo TGA2 thermobalance

4.3.4 Dynamic Mechanical Analysis (DMA)

Dynamic Mechanical Analysis was performed to evaluate the thermomechanical properties of the obtained materials. TA instruments DMA 850 (**Figure 12**) was used with tension film clamp. The analysed samples were prismatic specimens measuring 3.7 mm in width and 0.5 mm in thickness, subjected to a deformation of 0.1% at a frequency of 1 Hz. A temperature range of 3ºC·min^{-1} was applied from 20ºC to 200ºC.

Figure 12. TA instruments DMA 850

4.3.5 Infrared Spectroscopy (IR)

Infrared analysis was used to verify the complete conversion of methacrylate groups and to verify the presence of certain functional groups. The results are presented in transmittance (%) vs wavenumber (cm^{-1}).

The instrument employed was a Vertex 70 spectrometer (**Figure 13**), equipped with attenuated total reflectance (ATR) and a temperature-stabilizer FR-DGTS detector, offering a resolution of 4 cm^{-1}. A full spectrum can be acquired in the mid- and far- IR range from 6000 cm^{-1} to 50 cm^{-1}. Data processing was performed using the OPUS/IR software. Only a small sample quantity is required for analysis.

Figure 13. Vertex 70 spectrometer

4.3.6 Stress relaxation test

The same specimens and instrument used for DMA were employed for the stress relaxation test. The objective of the stress relaxation test is to determine whether the materials showed vitrimeric behaviour. Samples were equilibrated at 160ºC, then a constant deformation of 1% was applied and the stress (σ) necessary to maintain this deformation was monitored over time. From these experiments, the characteristic relaxation time τ can be obtained as the time necessary to obtain a stress relaxation of $\sigma(t)/\sigma_0 = 36.7$ %.

5 RESULTS AND DISCUSSION

[redacted]

To obtain the desired monomer two synthetic routes have been followed[12,14,15] (**Scheme 6, Scheme 7**).

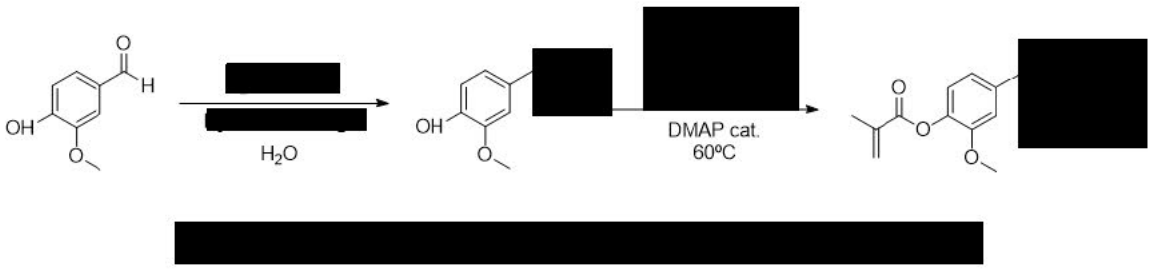

The process began with the synthesis of [redacted] following a procedure already described.[12] This step is straightforward as it is an easy synthesis, uses water as solvent which is a sustainable solvent ensuring environmental friendliness. In addition, purification is simple obtaining the product with a high purity and the yield of the reaction is good. These advantages make this synthesis highly scalable due to its ease.

Once the [redacted]. To do so, the [redacted] was reacted with [redacted] in the presence of DMAP as a catalyst towards a nucleophilic acyl substitution where the [redacted] The progress of the reaction was monitored through ^{1}H NMR spectroscopy.

The obtained ^{1}H NMR spectrum (**Figure 14**) shows a displacement [redacted] In addition to the expected product signals (the ones highlighted in blue); unexpected signals appeared (the ones highlighted in green). These signals were attributed to a byproduct formed during the reaction.

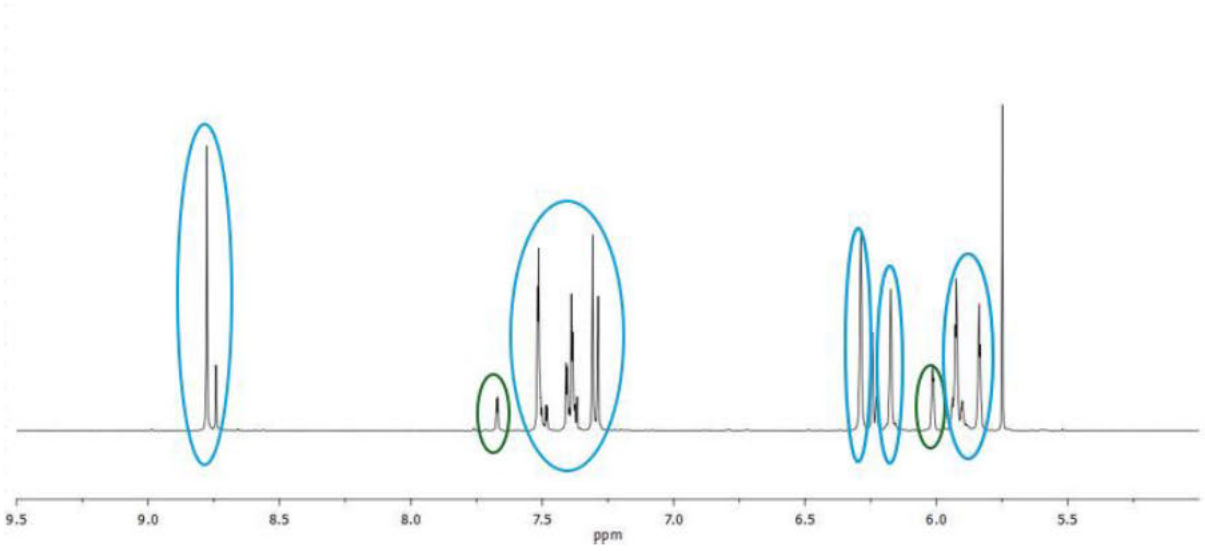

Figure 14. ^{1}H NMR spectrum of [redacted] in dmso-d_6. Fragment 5.0-9.5 ppm

It was suspected that this byproduct was a [redacted] While this typically occurs at high temperatures

(known as thermal dehydration), which was not the case here, it can also happen at lower temperatures in the presence of a catalyst—matching our reaction conditions (60ºC in the presence of DMAP).

To confirm this hypothesis, IR (**Figure 15**) and ^{13}C NMR (**Figure 16**) spectroscopy were performed [redacted] The detection of this group would support the formation of the proposed [redacted].

Looking at the IR spectrum (**Figure 15**) different bands could be observed. A clear band was observed around 3000 cm^{-1} corresponding to =C-H stretching and, another clear band was observed at 1700 cm^{-1} corresponding to C=C stretching. These two previously mentioned bands confirmed the formation of the reaction product, as they indicate the presence of a vinylic system. [redacted]

[redacted]

[redacted]

Therefore, based on the information obtained from both spectroscopic techniques, the initial hypothesis was considered true.

To address this issue, an alternative synthetic route (**Scheme 7**) has been proposed. This approach offers the advantage of operating under room temperature conditions, [redacted].

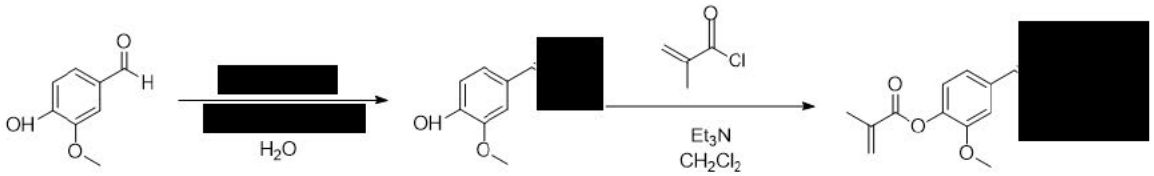

Scheme 7. Synthesis of the [redacted]

In this synthetic route, [redacted] reacts with methacryloyl chloride, a highly reactive compound, via a nucleophilic acyl substitution. The used methacryloyl chloride has been previously synthesised (**Scheme 3**) and it is purified through distillation. [redacted]

Once the reaction was finished, a characterization was done by means of ^{1}H NMR and in the obtained spectrum unexpected signals at chemical shifts of 6.24, 6.01 and 1.94 ppm were observed, corresponding to the presence of methacrylic acid. This methacrylic acid

could be formed from the hydrolysis of methacryloyl chloride as this reactant was in excess. To remove methacrylic acid and the remaining methacryloyl chloride found in excess several washes were carried out. The goal was to react basic aqueous solutions with these compounds, forming water-soluble salts that could be removed through extraction. So, initially a 5% wt. bicarbonate aqueous solution was used for the first wash. However, as methacrylic acid was still present, additional washes were performed using a 10% wt. sodium hydroxide aqueous solution. The ^{1}H NMR spectrum after these several washes can be seen in **Figure 17**.

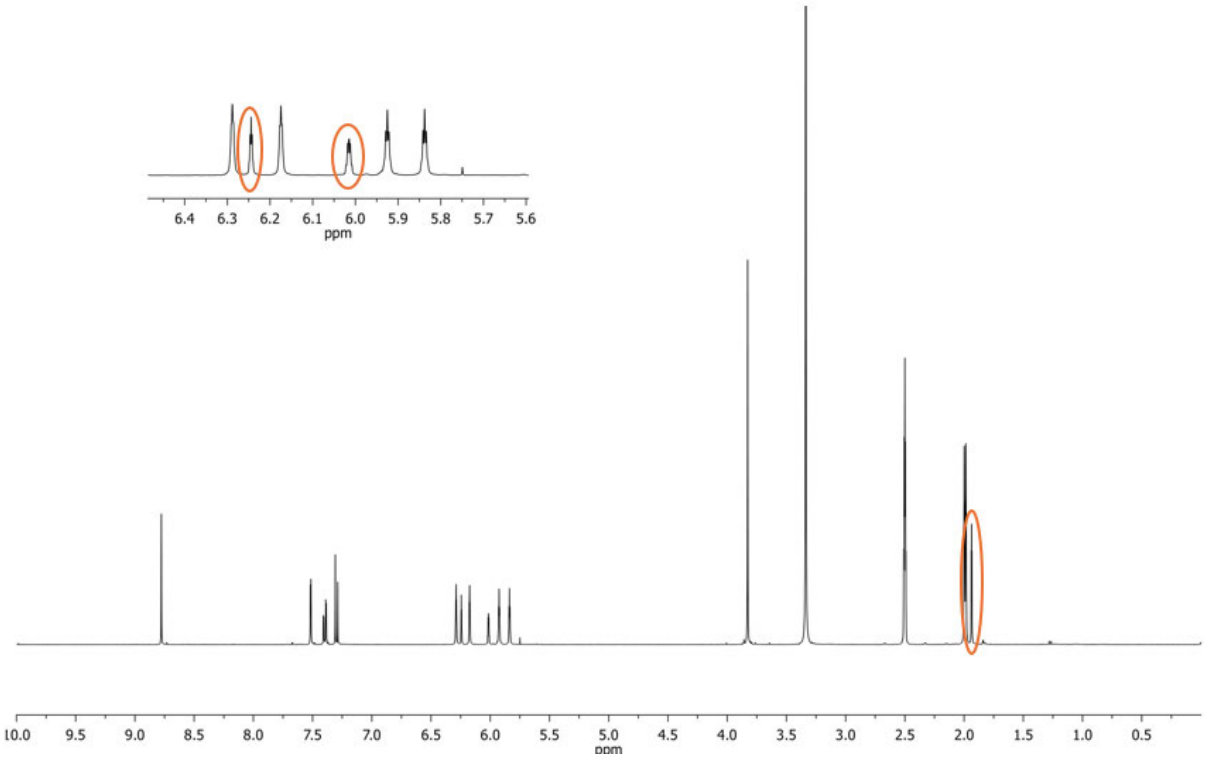

Figure 17. ^{1}H NMR spectrum of [redacted] after washes

After these last washes methacrylic acid was still present. Therefore, to purify the product of interest [redacted] another path was chosen.

The solid obtained from the reaction was dissolved in 65 mL of dichloromethane. Once it was completely dissolved it was added dropwise in a beaker which was filled with 650 mL of hexane and contained a magnetic stir bar. [redacted]

Once it has precipitated the solution mixture was transferred to a round bottom flask and it was located in the freezer overnight. The next day the solution was filtrated under vacuum and then, three washes were performed with cold hexane. After the washings the obtained product was placed in a watch glass in the vacuum oven to eliminate remaining hexane. Obtaining a 56% of yield.

The final product was characterized by ^{1}H NMR (**Figure 18**), yielding a clear and pure spectrum with no signal corresponding to the byproduct. This is a significant result, as it indicates that this alternative synthetic route successfully produces the desired monomer without generating the unwanted byproduct.

The DSC analysis (**Figure A11**) determined a melting temperature (T_m) of 100ºC for the [redacted]

5.2 Synthesis of guaiacol methacrylate monomer

For this synthesis, two synthetic routes were followed[14,15] (**Scheme 8, Scheme 9**).

The first approach (**Scheme 8**) involved reacting guaiacol with [redacted] in the presence of DMAP. While this method was effective, its main drawback was the excessive reaction time. Initially, the mixture was maintained at room temperature for three hours, followed by a prolonged reaction period of at least 24 hours at 70ºC. After this time, thin-layer chromatography (TLC) was used to monitor the reaction, employing a hexane and ethyl acetate mixture (6:1) as the mobile phase. The TLC results indicated that guaiacol was still present, suggesting incomplete conversion. Consequently, the reaction was extended for another 24 hours and [redacted] was added to the reaction mixture. Even after 48 hours, TLC results remained unchanged. Further analysis through ^{1}H NMR revealed that the reaction had reached approximately 80% conversion. Although this was a reasonable conversion, the lengthy process made it impractical.

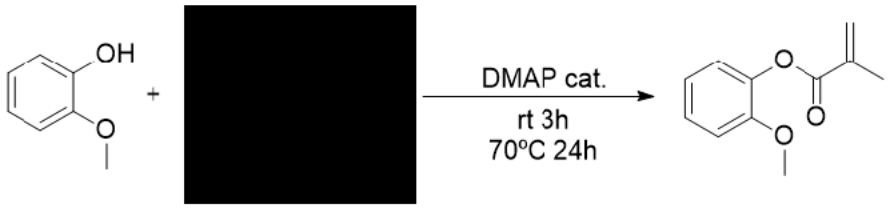

Scheme 8. Synthesis of guaiacol methacrylate (Meta-Guai)

To address this limitation, an alternative synthetic route (**Scheme 9**) was implemented. In this method, guaiacol was reacted with the previously synthetized methacryloyl chloride to obtain a complete conversion.

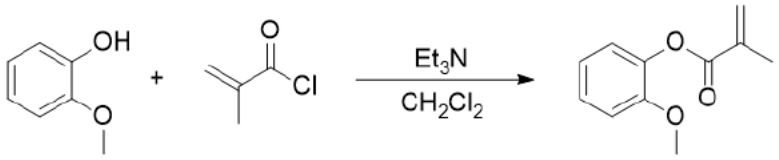

Scheme 9. Synthesis of guaiacol methacrylate (Meta-Guai)

This second synthetic route successfully yielded guaiacol methacrylate while significantly reducing reaction time, resolving the challenges associated with the first synthetic route.

5.3 Preparation of the material

[redacted]

The formulations were irradiated with a UV lamp operating between 365 nm and 405 nm for 5 minutes. As the photoinitiator used was BAPO (**Figure 19**) which has a maximum absorption wavelength around 405 nm[17], this range was suitable for photopolymerization.

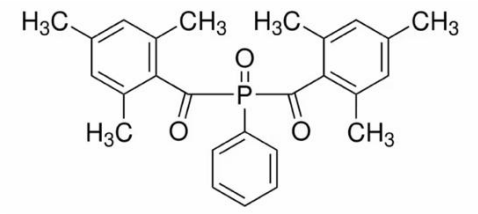

Figure 19. Phenylbis(2,4,6-trimethylbenzoyl)-phosphine oxide structure

After photopolymerization, a post-curing process of 1 hour at 160ºC was done to ensure the reaction reached completion as during the initial curing, not all reactive groups may fully react, especially if the cure is done at lower temperatures or for shorter times (which is our case). The post curing step enhances the crosslinking density, which restricts the mobility of the polymer chains and as a consequence implies an increase in the glass transition temperature (T_g). In **Figure 20**, the yellowish obtained material after the post curing step can be seen.

Figure 20. Yellowish obtained material

Figure A12 shows the T_g for each of the prepared formulations after the post-curing. These temperatures are considered optimal for 3D printing applications.

5.3.1 Thermal stability

The thermal stability of the cured samples was studied by thermogravimetric analysis. This analysis provides two different graphs, (**Figure 21**) shows the TGA curve and (**Figure 22**) shows the first derivative of TGA curve.

This analysis had only been done for the 25/75 formulation.

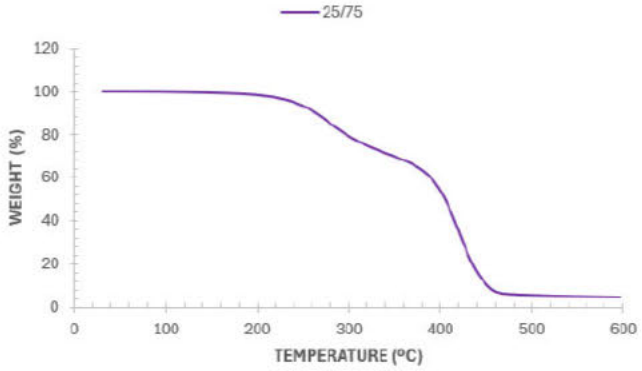

Figure 21. TGA curve

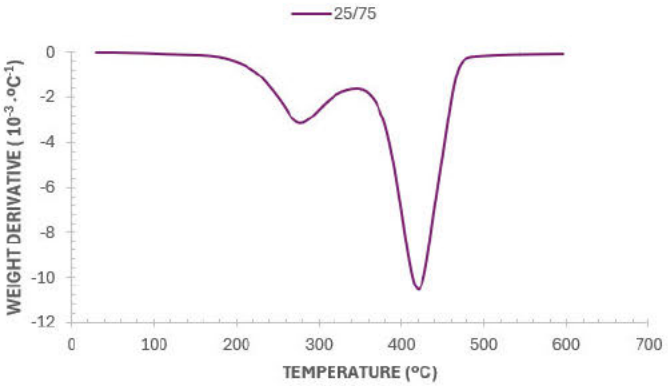

Figure 22. TGA 1st derivative curve

In **Table 4**, is summarized the data extracted from the TGA graphs.

Table 4. Calorimetric data of the curing process and temperature of 2% of weight loss in an N_2 atmosphere of the 25/75 formulation.

[redacted]

5.3.2 Thermomechanical characterization

In terms of thermomechanical characterization, analysis was conducted using dynamic mechanical analysis. The measurements provided values for tan δ and for the storage modulus (E').

Figures 23 and **24** present tan δ and E' as a function of temperature [redacted]

In **Figure 23**, [redacted] shows a glass transition temperature of 132ºC, whereas [redacted] shows a significant lower glass transition temperature (97ºC). [redacted] **Figure 23** provides additional insight into material composition through peak shape analysis. A narrow and a high peak corresponds to a homogeneous and ordered structure, while broad and short peaks indicate the disordered network. The presence of both peak types suggests that the obtained materials exhibit distinct structural properties.

This difference is further confirmed by analysing the storage modulus (**Figure 24**). [redacted]

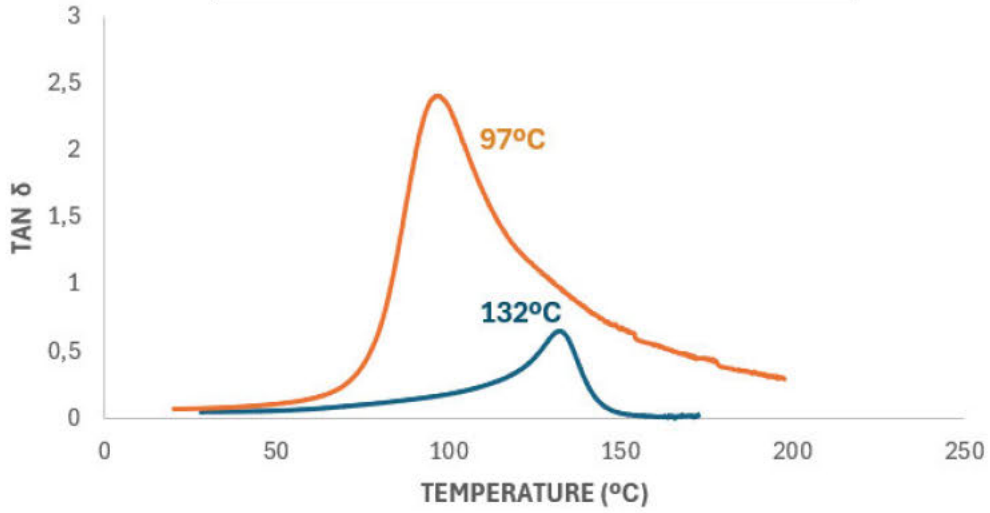

Figure 23. Tan δ graph

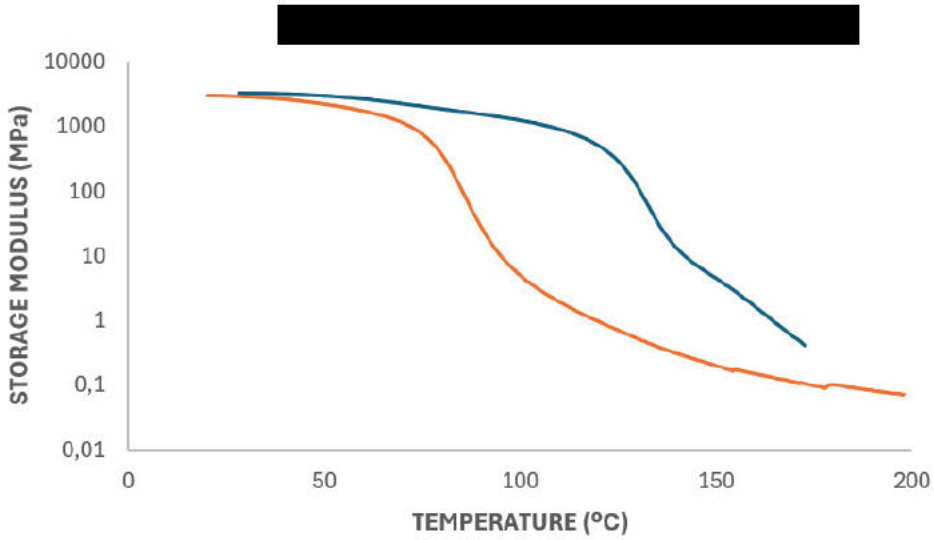

Figure 24. Storage modulus graph

5.3.3 Vitrimeric character

The vitrimeric character of the obtained material was studied through stress relaxation test using DMA.[9]

[redacted]

The stress relaxation behaviour [redacted] is shown in the **Figure 25**. Stress relaxation, represented by the decay of normalized stress ($\sigma(t)/\sigma_0$) over time, provides insight into the dynamic rearrangement capability of the polymer network under constant strain.

[redacted]

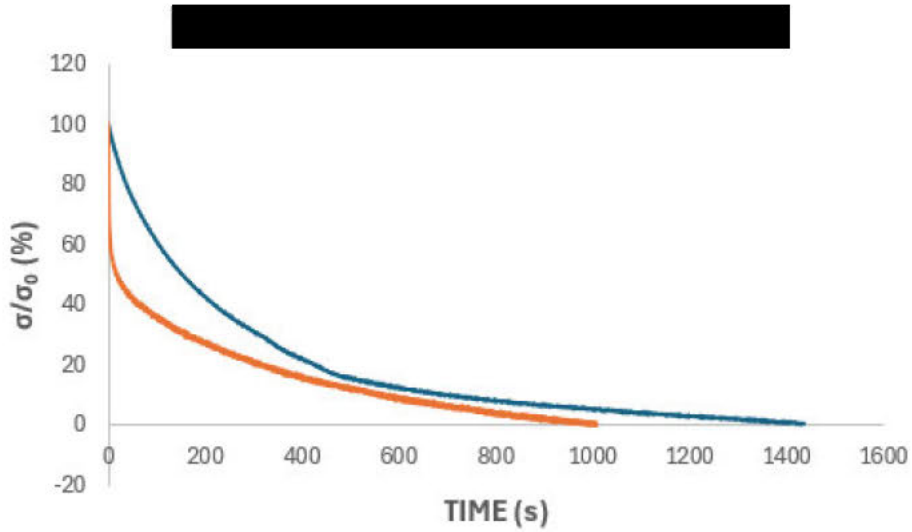

Figure 25. Stress relaxation test

6 CONCLUSIONS

This research successfully demonstrates the synthesis and characterization of a new vitrimeric material derived from vanillin, a renewable aromatic compound. The alternative synthetic route employing methacryloyl chloride proved to be more effective, ensuring purity and reproducibility.

The photopolymerization process, confirmed through infrared spectroscopy, revealed the complete conversion of methacrylate groups, validating the efficiency of the selected photoinitiator under UV irradiation.

Differential Scanning Calorimetry (DSC) confirmed glass transition temperatures ranging between 85ºC and 97ºC, ensuring adequate thermal performance for applications such as 3D printing.

Dynamic Mechanical Analysis (DMA) showcased significant structural differences in the obtained material.

Stress relaxation test demonstrates that the material relaxes faster with the presence of a catalyst.

6.1 FUTURE WORK

Looking ahead, exploring the potential of these materials for use in 3D printing would be a valuable direction for future research. Additionally, studying the materials flow behavior, crosslinking dynamics, and structural integrity under printing conditions would provide deeper insight into their suitability for advanced manufacturing applications.

7 BIBLIOGRAPHY

(1) Fache, M.; Boutevin, B.; Caillol, S. Vanillin Production from Lignin and Its Use as a Renewable Chemical. *ACS Sustain Chem Eng* **2016**, *4* (1), 35–46. https://doi.org/10.1021/acssuschemeng.5b01344.

(2) Jagadish, R. S.; Divyashree, K. N.; Viswanath, P.; Srinivas, P.; Raj, B. Preparation of N-Vanillyl Chitosan and 4-Hydroxybenzyl Chitosan and Their Physico-Mechanical, Optical, Barrier, and Antimicrobial Properties. *Carbohydr Polym* **2012**, *87* (1), 110–116. https://doi.org/10.1016/j.carbpol.2011.07.024.

(3) Amarasekara, A. S.; Razzaq, A. Vanillin-Based Polymers—Part II: Synthesis of Schiff Base Polymers of Divanillin and Their Chelation with Metal Ions. *ISRN Polymer Science* **2012**, *2012*, 1–5. https://doi.org/10.5402/2012/532171.

(4) Rao, V. S.; Samui, A. B. Structure-Property Relationship of Photoactive Liquid Crystalline Polyethers Containing Benzylidene Moiety. *J Polym Sci A Polym Chem* **2009**, *47* (8), 2143–2155. https://doi.org/10.1002/pola.23303.

(5) Post, W.; Susa, A.; Blaauw, R.; Molenveld, K.; Knoop, R. J. I. A Review on the Potential and Limitations of Recyclable Thermosets for Structural Applications. *Polymer Reviews*. Taylor and Francis Inc. April 2, 2020, pp 359–388. https://doi.org/10.1080/15583724.2019.1673406.

(6) Berne, D.; Laviéville, S.; Leclerc, E.; Caillol, S.; Ladmiral, V.; Bakkali-Hassani, C. How to Characterize Covalent Adaptable Networks: A User Guide. *ACS Polymers Au* **2025**. https://doi.org/10.1021/acspolymersau.5c00004.

(7) Denissen, W.; Winne, J. M.; Du Prez, F. E. Vitrimers: Permanent Organic Networks with Glass-like Fluidity. *Chem Sci* **2016**, *7* (1), 30–38. https://doi.org/10.1039/c5sc02223a.

(8) Zheng, J.; Png, Z. M.; Ng, S. H.; Tham, G. X.; Ye, E.; Goh, S. S.; Loh, X. J.; Li, Z. Vitrimers: Current Research Trends and Their Emerging Applications. *Materials Today*. Elsevier B.V. December 1, 2021, pp 586–625. https://doi.org/10.1016/j.mattod.2021.07.003.

(9) Verdugo, P.; Santiago, D.; De la Flor, S.; Serra, À. A Biobased Epoxy Vitrimer with Dual Relaxation Mechanism: A Promising Material for Renewable, Reusable, and Recyclable Adhesives and Composites. *ACS Sustain Chem Eng* **2024**, *12* (15), 5965–5978. https://doi.org/10.1021/acssuschemeng.4c00205.

(10) Pettazzoni, L.; Ximenis, M.; Leonelli, F.; Vozzolo, G.; Bodo, E.; Elizalde, F.; Sardon, H. Oxime Metathesis: Tuneable and Versatile Chemistry for Dynamic Networks. *Chem Sci* **2024**, *15* (7), 2359–2364. https://doi.org/10.1039/d3sc06011j.

(11) Krishnakumar, B.; Sanka, R. V. S. P.; Binder, W. H.; Parthasarthy, V.; Rana, S.; Karak, N. Vitrimers: Associative Dynamic Covalent Adaptive Networks in Thermoset Polymers. *Chemical Engineering Journal*. Elsevier B.V. April 1, 2020. https://doi.org/10.1016/j.cej.2019.123820.

[redacted]

(13) Veličić, Z.; Rusmirović, J.; Prlainović, N.; Tomić, N.; Veličković, Z.; Taleb, K.; Marinković, A. D. The Optimization of Glycidyl Methacrylate Based Terpolymer Monolith Synthesis: An Effective Candida Rugosa Lipase Immobilization Support. *Journal of Polymer Research* **2020**, *27* (5). https://doi.org/10.1007/s10965-020-02127-z.

(14) Dworak, C.; Liska, R. Alternative Initiators for Bimolecular Photoinitiating Systems. *J Polym Sci A Polym Chem* **2010**, *48* (24), 5865–5871. https://doi.org/10.1002/pola.24396.

(15) Stanzione, J. F.; Sadler, J. M.; La Scala, J. J.; Wool, R. P. Lignin Model Compounds as Bio-Based Reactive Diluents for Liquid Molding Resins. *ChemSusChem* **2012**, *5* (7), 1291–1297. https://doi.org/10.1002/cssc.201100687.

(16) Li, R.; Shi, J.; Zhou, X.; Li, Z.; Zhao, Y.; Liu, Z.; Wang, J. Green Synthesis of Nitriles from Biomass-Derived Aldehydes by Evoking Intrinsic Cooperative Effects of Ionic Liquids. *ACS Sustain Chem Eng* **2024**, *12* (30), 11338–11346. https://doi.org/10.1021/acssuschemeng.4c03533.

(17) Qin, H.; Yang, D.; Zhao, J.; Leng, J.; Zhang, J.; Zhang, Y.; Hao, M.; Cui, J.; Yuan, H. Effect of Substitution on Light-Curable Properties in Diphenyl(2,4,6-Trimethylbenzoyl)Phosphine Oxide: DFT and TD-DFT Calculations. *Mater Today Commun* **2023**, *35*. https://doi.org/10.1016/j.mtcomm.2023.106071.

8 APPENDIX

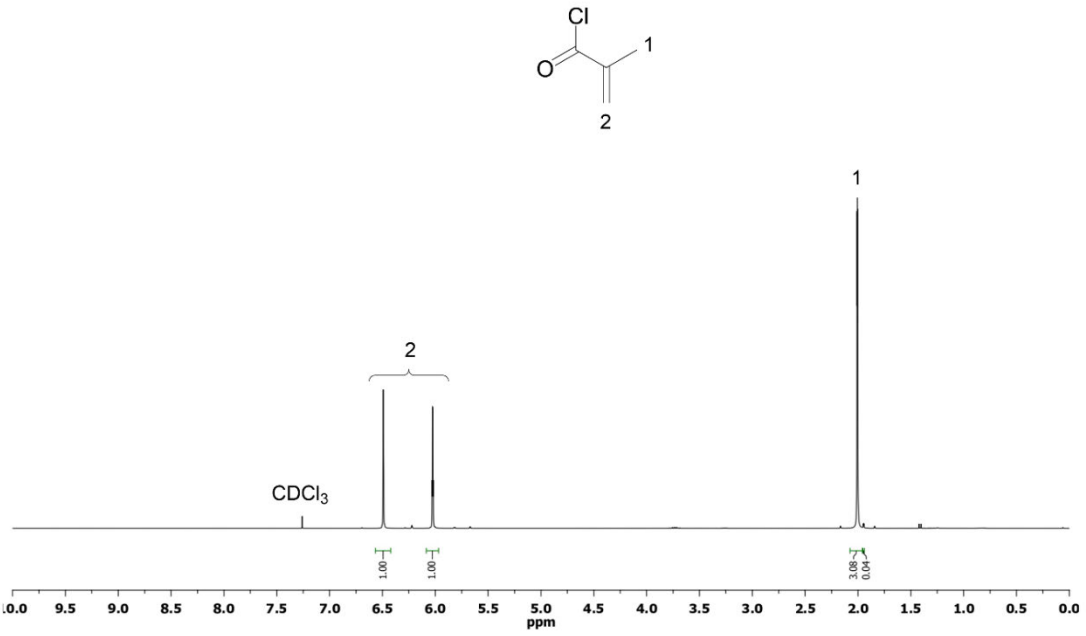

Figure A3. ^{1}H NMR of methacryloyl chloride in $CDCl_3$

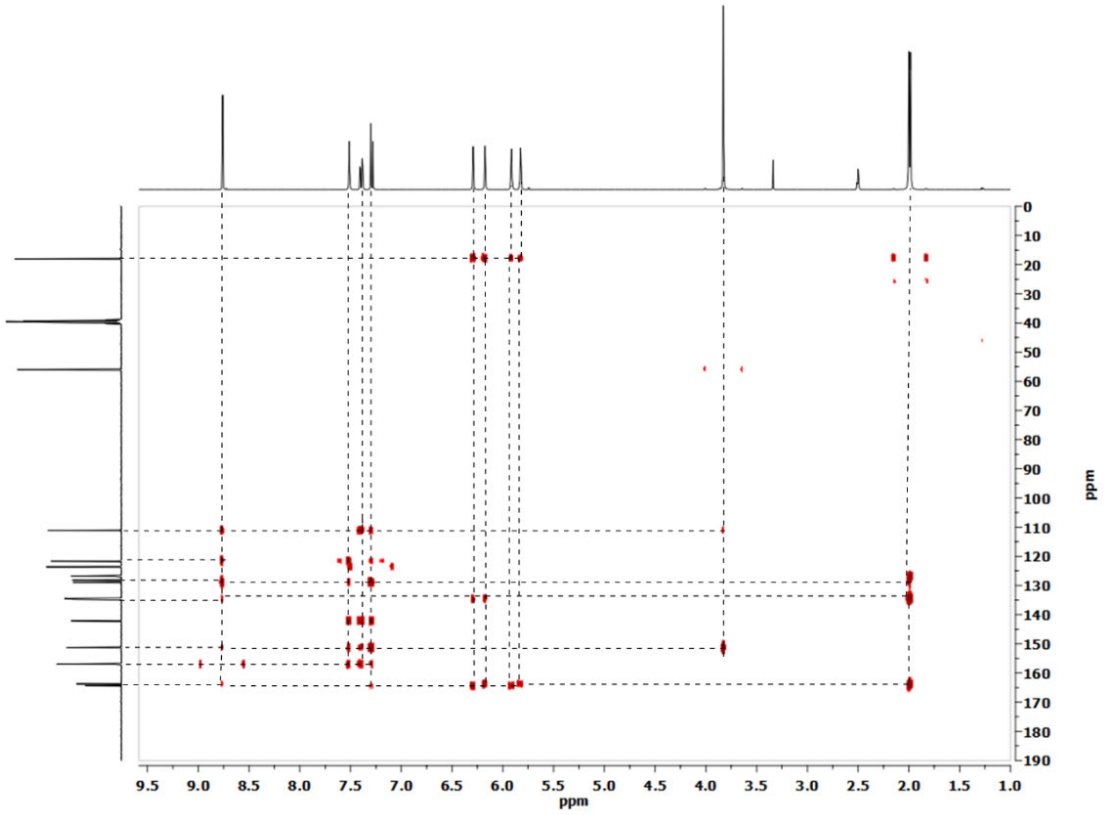

Figure A5. HMBC of [redacted]) in dmso-d_6

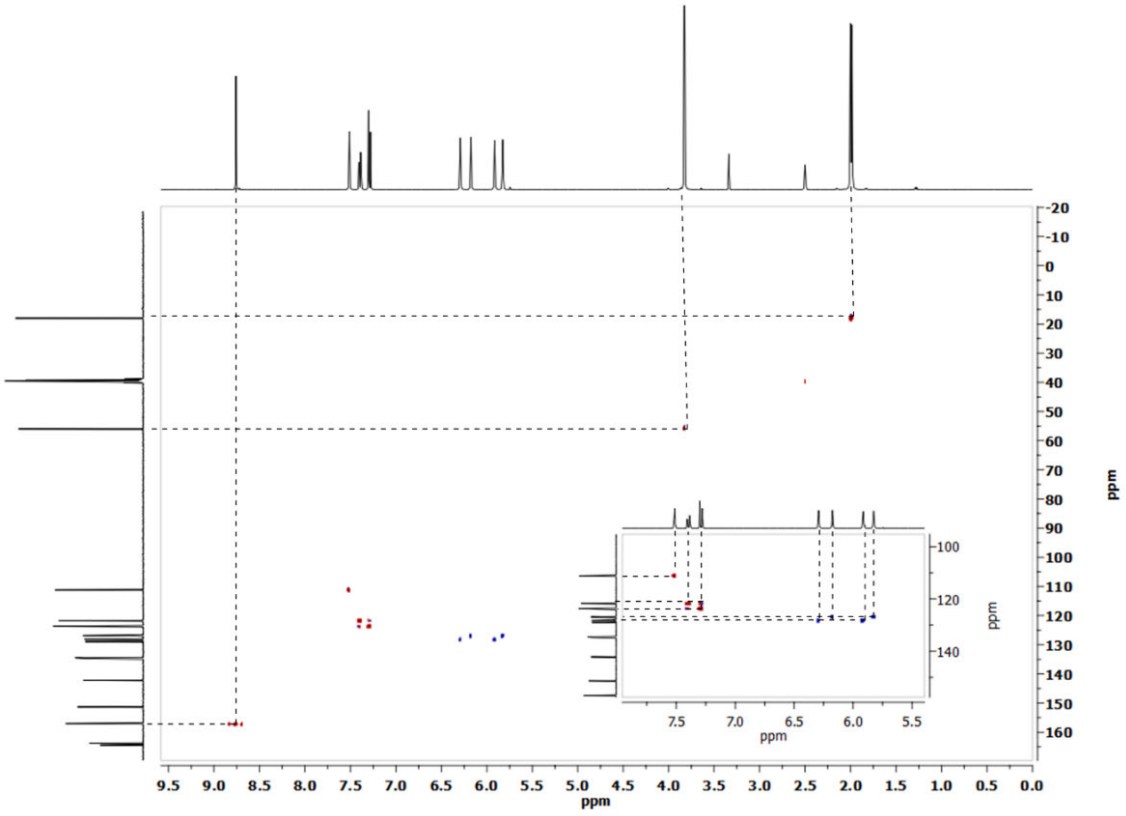

Figure A6. HSQC of [redacted] in dmso-d_6

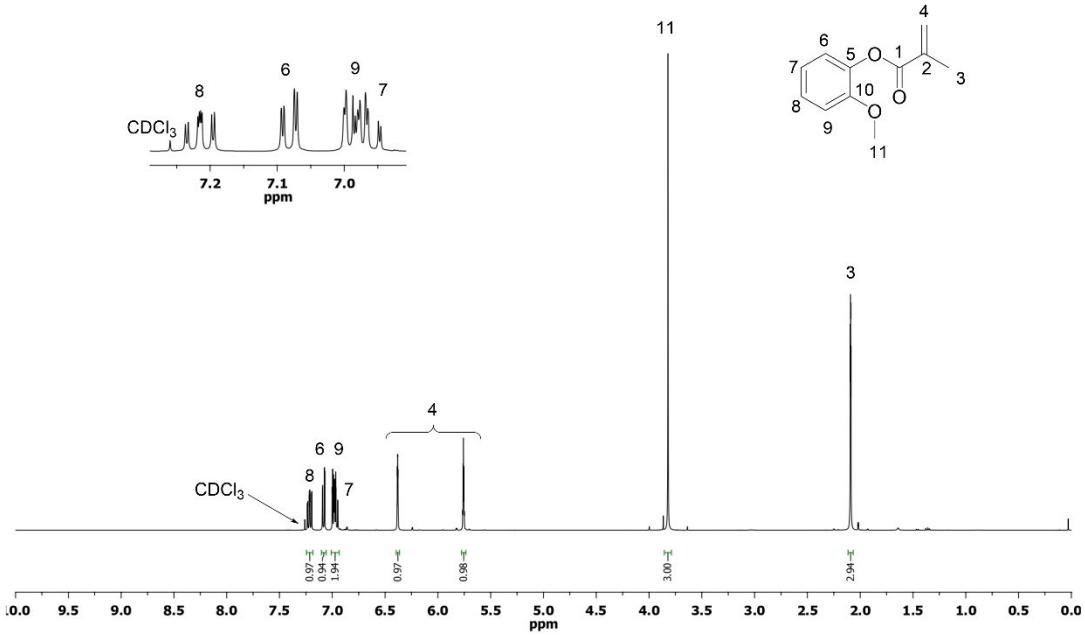

Figure A7. ^{1}H NMR of guaiacol methacrylate (Meta-Guai) in $CDCl_3$

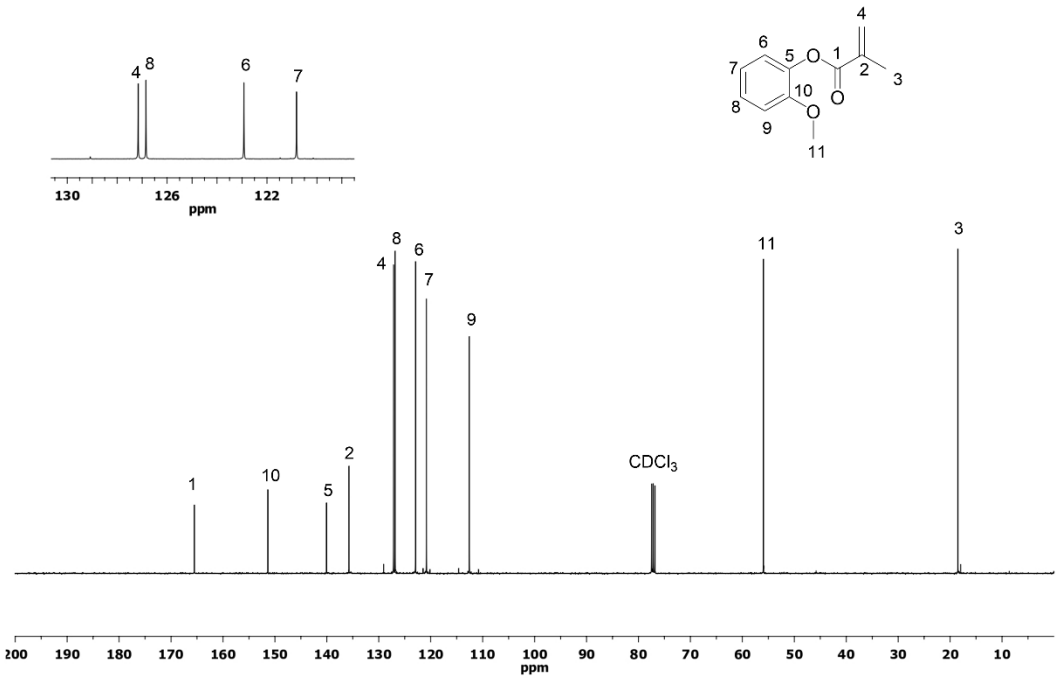

Figure A8. ^{13}C NMR of guaiacol methacrylate (Meta-Guai) in $CDCl_3$

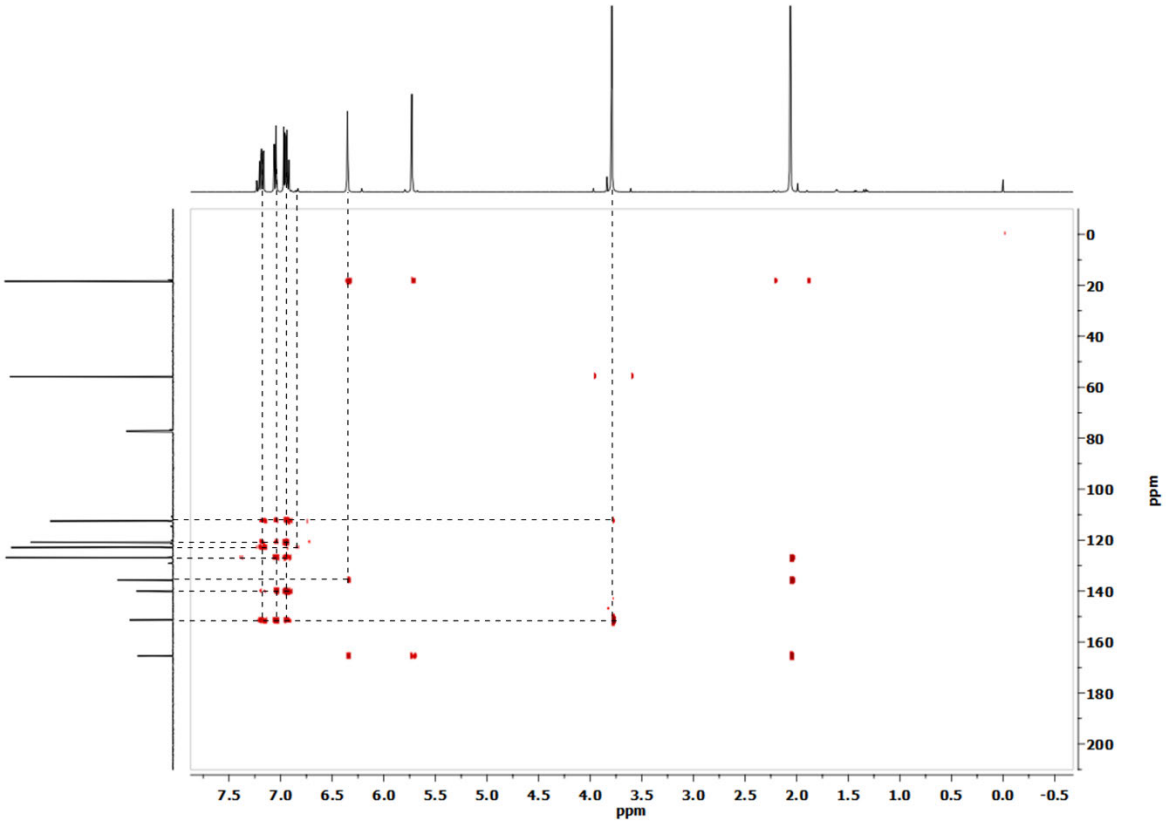

Figure A9. HMBC of guaiacol methacrylate (Meta-Guai) in $CDCl_3$

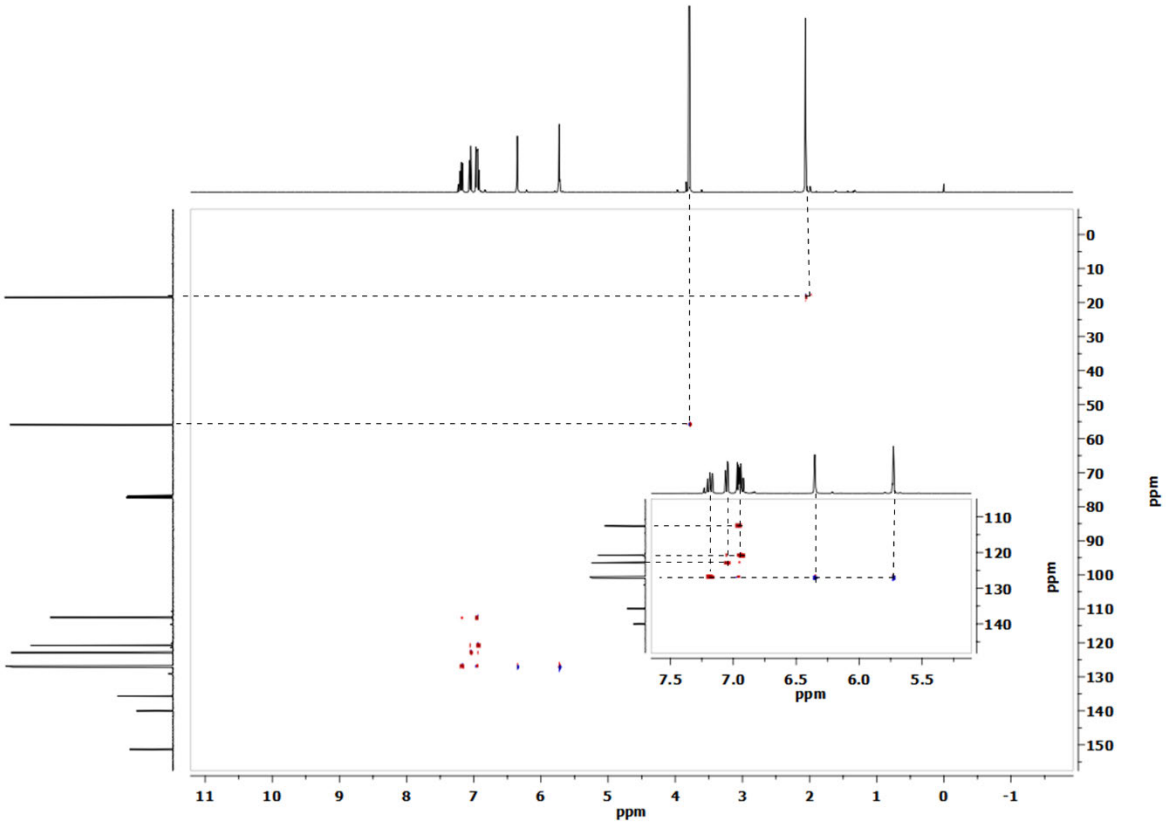

Figure A10. HSQC of guaiacol methacrylate (Meta-Guai) in $CDCl_3$